# Statics and dynamics of radial nematic liquid-crystal droplets manipulated by laser tweezers

Etienne Brasselet
*Laboratoire CPMOH Université Bordeaux 1, CNRS, 351 Cours de la Libération, 33405 Talence Cedex, France*

Naoki Murazawa, Saulius Juodkazis, and Hiroaki Misawa
*Research Institute for Electronic Science, Hokkaido University, N21W10 CRIS Bldg., Sapporo 001-0021, Japan*
(Received 24 January 2008; published 15 April 2008)

Laser manipulation of trapped radial 4′-n-pentyl-4-cyanobiphenyl (5CB) nematic liquid-crystal droplets induced by molecular reordering is presented. We show experimentally that optical tweezers having linear, elliptical, or circular polarization can break the radial symmetry of the initial molecular organization inside a radial nematic droplet. Static distorted or twisted deformation modes and steady or unsteady nonlinear rotational dynamics are observed. Statics results are analyzed in terms of light-induced radial or left-right symmetry breaking effects associated with optical reorientation. The dynamical observations are compared with simulations from a slab analog model, for which orientational processes driven by optical nonlinearities can be accurately described. This study confirms that light-induced bulk reordering is an essential ingredient towards the understanding of the behavior of radial nematic liquid-crystal droplets in laser tweezers, as suggested by previous studies.

DOI: 10.1103/PhysRevE.77.041704 PACS number(s): 61.30.Pq, 61.30.Gd, 42.70.Gi

## I. INTRODUCTION

Laser trapping and manipulation of microparticles or nanoparticles and materials is used in the determination of optical and mechanical properties as well as for their tracking, sorting, deposition, or structural control [1–11]. Liquid-crystal (LC) materials are well suited for laser manipulation due to their high refractive index and birefringence. In addition, the high potential of interest of LCs in biomedical applications [12] might benefit from their optical manipulation versatility. Among possible spatially confined LC systems that can be manipulated in laser tweezers, droplets suspended in a surrounding nonmiscible fluid (generally water) appear as a benchmark geometry to study trapping, displacement and angular manipulation in various mesophases such as nematic [13,14], smectic [15], or cholesteric LCs [16]. In these systems the bulk molecular ordering is highly sensitive to surface effects, which was exploited in Ref. [17] where the addition of a surfactant in a solution containing initially bipolar nematic LC droplets was shown to induce to bulk realignment leading to the formation of radial droplets. Many different droplet configurations that depend on the mesophase can be found [18–20], which enrich much the light-matter interaction in laser tweezers compared to the case of solid birefringent particles.

Similar to an earlier demonstration using birefringent calcite particles [21], LC birefringent droplets can be continuously rotated by light when the latter deposits angular momentum while passing through it. However, there are many possible mechanisms leading to effective rigid body rotation of such a LC droplet by a laser beam. One can mention the optical torque transfer through wave plate behavior [13,14], light scattering [14,22], photon absorption processes [14], or optical realignment based on optical orientational nonlinearities [23] inside the droplet [17,24]. These features make LC droplets useful for microrheology measurements by relating the averaged rotation frequency of a spinning droplet to the surrounding medium viscosity [25,26]. Optomechanical switching has been demonstrated to be another potential application of light-driven rotating LC droplets [27]. However, material information can also be extracted from instantaneous rotation frequency of a rotating droplet as shown in Ref. [28] where the Brownian motion of a rotating nematic droplet was studied. The role played by the polarization of the beam that induces the rotational motion requires specific attention. Indeed, although there is not much surprise in observing birefringent LC droplet rotation using elliptically or circularly polarized laser tweezers, intriguing rotational behavior has been observed in large pitch cholesterics using linearly polarized light [16], which remains unexplained, and nontrivial photoinduced rotational effects were predicted in the presence of a small amount of dye added in a nematic droplet [29].

Liquid-crystal defects and structures are other classes of confined LC objects that can be directly manipulated using laser tweezers. This was achieved in nematic [30], smectic [31], and cholesteric [32,33] mesophases. Such an approach differs from the indirect manipulation of defects and structures using an optically trapped solid particle [34], which is actually related to the general problem of laser trapping in anisotropic fluids [35]. Direct optical manipulation has been revealed useful to determine *in situ* material properties, such as line tension of disclination lines [32]. Moreover, it was shown that orientational optical nonlinear effects can lead to significant deformations of LC structures at high trapping power [33].

In this work we show that the main features of laser-induced molecular realignment inside the micrometer-sized LC radial nematic droplets under linearly, elliptically, or circularly polarized laser tweezers can be grasped from simple models that take into account both the wave plate behavior and optical orientational nonlinearities of LCs. Statics in-plane and twisted regimes are analyzed in terms of light-induced radial and left-right symmetry breaking effects associated with optical reorientation. Moreover, dynamical regimes are compared with a corresponding slab analog

 

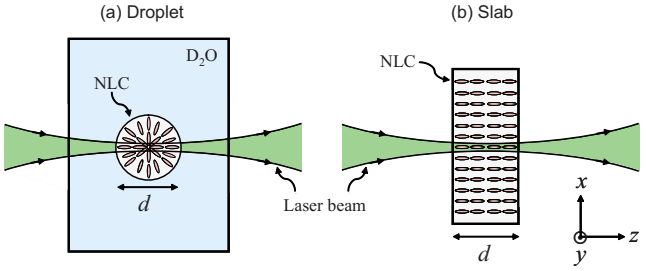


FIG. 1. (Color online) Illustration of (a) the radial nematic LC droplet of diameter $d$ held in heavy water by laser tweezers and (b) the nematic LC slab analog with thickness $d$ with homeotropic boundary conditions.

model, for which orientational processes driven by optical nonlinearities can be accurately described [36,37]. We demonstrate that former experimental results on radial droplets dynamics are qualitatively described by such a simple model, thus pointing out the optical orientational nonlinearity as an essential ingredient of observed phenomena, as suggested by previous studies.

## II. EXPERIMENTS AND SLAB ANALOG

Nematic liquid-crystal 4′–n–pentyl–4–cyanobiphenyl (5CB) was dispersed in heavy water ($D_2O$) for laser manipulation. The $D_2O$ was used to avoid significant temperature rise due to high laser power irradiation, which is approximately 10 times smaller than in the $H_2O$. The cationic surfactant hexadecyltrimethylammonium bromide, was added at a concentration $c=41.2$ $\mu$M higher than the critical micelle concentration ($c_{\mathrm{mic}} \sim 13$ $\mu$M) to obtain all droplets with radial molecular alignment.

Laser trapping and manipulation of radial droplets were carried out using a YAG CW laser operating at wavelength $\lambda=1064$ nm and a microscope [17]. The laser trap was set with a high numerical aperture (NA) objective lens, NA $=1.3$. The polarization state of the trapping beam was precisely controlled by a pair of wave plates. Statics distorted regimes were analyzed using polariscope imaging, and rotational dynamics of droplets was monitored by polarization changes of the laser trapping beam after passing through the droplet [17].

Since the beam diameter is a few times smaller than droplet radius in our experiments, we suggest one retrieves some information about experimental laser manipulation of a radial droplet with diameter $d$ from the knowledge of optically induced reorientation of a homeotropically aligned nematic LC slab with thickness $d$, as depicted in Fig. 1. Note that the comparison of the behavior of a radial droplet and its slab analog can only be considered as qualitative and may serve as a guide for a future three-dimensional (3D) model that should be taken into account for the particular 3D geometry of the manipulated object. In particular, while the droplets can rotate in a low viscosity water (compared to LC) there is no exterior environment other than the 5CB LC in the slab case, thus preventing any quantitative comparison between observed and predicted rotation frequency. Since the first observation of light-induced collective molecular rotation in a nematic LC film [38] many attempts to derive slab models able to describe optically induced nonlinear reorientation dynamics under circular or elliptical polarization have been performed within the plane wave approximation [39–41]. A complete and rigorous plane wave model has been obtained a few years ago, which evidences many kinds of dynamical regimes and secondary instabilities above the Fréedericksz transition threshold [36,37]. We further use the later model when comparing rotational droplet dynamics with the slab analog geometry.

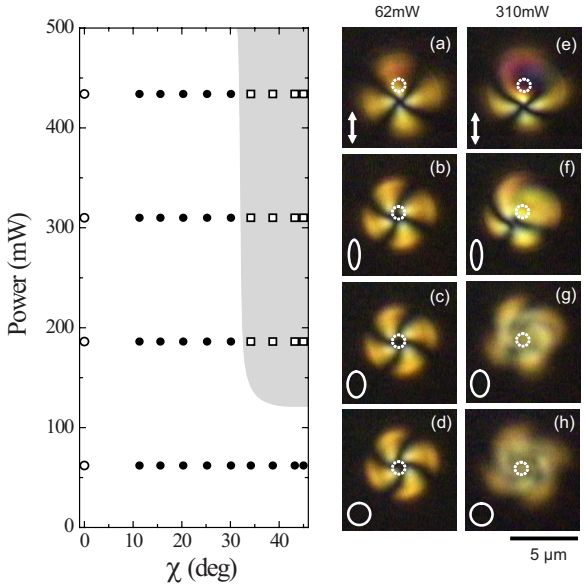


FIG. 2. (Color online) Left: map of laser-induced molecular reordering in the $(\chi,P)$ plane of parameters. Circles: static untwisted (open symbol) and twisted (filled symbol) distorted states; Squares: rotating regimes. The gray area is a guide for the eye. Right: polariscope images of a 6-$\mu$m-diam droplet for increasing ellipticity at trapping power $P=62$ mW [(a)–(d)] and $P=310$ mW [(e)–(h)]. The angle $\chi$ is 0°, 25.2°, 34.2°, and 45° for panels (a)–(d) and (e)–(h), respectively. The dashed circle indicates the locus of the focal spot.

## III. RESULTS AND DISCUSSION

Figure 2 summarizes the observed reorientation regimes of a 5CB radial droplet in the plane of parameters $(\chi,P)$. The angle $\chi$ refers to a laser tweezers polarization state, which is determined by the ellipticity angle $\chi$ defined as $\tan\chi = \pm b/a$, where $a$ and $b$ correspond to the major and the minor axis of the polarization ellipse. Therefore $\chi=0$ and $\pm\pi/4$ hold for linear and (left- or right-handed) circular polarization, respectively. The power $P$ is the total incident power onto the droplet. Various distinct regimes, statics or dynamical, are found and identified by visual inspection of polariscope images (see Fig. 2) and/or polarization analysis of the laser beam at the output of the droplet. More precisely, three regimes are obtained and correspond either to in-plane or twisted distorted reordering or to rotational motion of droplets. In terms of symmetry of internal molecular align-

ment four cases emerge in terms of laser tweezers polarization: (i) linear polarization case, associated with radial symmetry breaking (SB) and statics distortions; (ii) weakly elliptical polarization case, associated with left-right SB and statics distortions; (iii) strongly elliptical polarization case, associated with left-right SB and rotational dynamics; and (iv) circular polarization case, associated with left-right SB and rotational dynamics. Although the last two cases look the same, it will be shown later that nonlinear rotational dynamics is different (see Fig. 12).

Further details are presented in the following sections where statics and quasistatics (Sec. III A) and dynamics (Sec. III B) are studied separately.

### A. Statics and quasistatics

Before trapping, the image of a radial droplet between crossed polarizers exhibits the characteristic extinction Maltese cross of a perfectly radial droplet. Once the droplet is trapped, this cross is perturbed correspondingly to optical molecular reordering inside the droplet, as illustrated in Figs. 2(a)–2(d). Two distinct cases are easily identified from distortions of the conoscopic dark crosses. A radial SB is observed for linearly polarized laser tweezers ($\chi=0$) while a left-right SB appears for elliptically polarized laser tweezers ($\chi\neq 0$). In all cases we conclude to an optical reordering, even at the smaller trapping powers, which practically means thresholdless reorientation.

The absence of a reorientation threshold is reminiscent of the initial radial structure of a droplet. Indeed, the optical torque $\mathbf{\Gamma}_{\text{opt}}$ exerted onto the director $\mathbf{n}$ is proportional to $\langle(\mathbf{n}\cdot\mathbf{E})(\mathbf{n}\times\mathbf{E})\rangle_t$, where $\mathbf{E}$ is the electric field of light and the brackets mean time averaging. Let us consider an initial situation where a radial droplet is perfectly centered with respect to the trapping beam. From a geometrical point of view $\mathbf{\Gamma}_{\text{opt}}=\mathbf{0}$ only for the optical ray that corresponds to the central part of the beam (where $\mathbf{n}$ and $\mathbf{E}$ are perpendicular) and $\mathbf{\Gamma}_{\text{opt}}\neq\mathbf{0}$ elsewhere. Nevertheless, a perfect centering leads to an overall null contribution due to radial symmetry. However, due to the finite extension of the laser beam, any residual imperfection will reveal a nonzero optical torque that leads to molecular reorientation through a thresholdless optical Fréedericksz transition [23]. Therefore we observe radial SB for linear polarization, and a left-right SB too for elliptical polarization resulting from angular momentum transfer, whatever the trapping power is.

#### 1. Radial symmetry breaking

In order to quantify the radial SB effects we define the off-centering length $\ell$ as the distance between the center of the trapping beam and the droplet center of mass (see the inset of Fig. 3). The dependence of $\ell$ on tweezers ellipticity is shown in Fig. 3 for several trapping powers. Light-induced radial SB is maximum for linear polarization and decreases monotonically as the ellipticity reaches $\chi=\pi/4$, where the tweezers are circularly polarized. At large ellipticity values we found $\ell\simeq 0$ within our experimental error. The polarization dependence of radial SB is related to the preferred realignment direction given by the major axis of the polarization ellipse. Indeed, the asymmetry due to elliptical polarization decreases with increasing ellipticity and tends toward zero when $\chi=\pi/4$ in correspondence with the behavior $\ell(\chi)$ shown in Fig. 3. On the other hand, the power dependence of radial SB is illustrated in Figs. 2(a) and 2(e) at $\chi=0$, which corresponds to a pure radial SB effect. The effect increases with power as shown by the volume expansion of the region where molecular alignment tends to be parallel to the input polarization. This may be used to operate quasistatics angular manipulation of a droplet by rotating the plane of polarization of the laser tweezers as illustrated in Fig. 4. Consequently, the angular manipulation of LC droplets is not restricted to bipolar ones. In addition, the angular precision of such a procedure only depends on polarization control and thus can be very accurate.

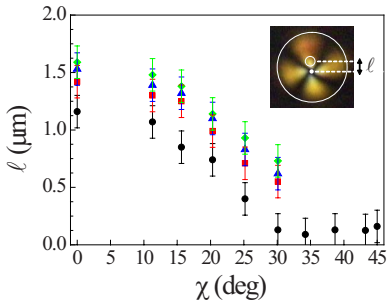


FIG. 3. (Color online) Off-centering distance as a function of ellipticity angle at trapping power $P=62$ mW (circles), $P=186$ mW (squares), $P=310$ mW (triangles), and $P=432$ mW (diamonds) for the situation that corresponds to Fig. 2. Inset: definition of $\ell$. The outer circle, the inner circle, and the dot indicate, respectively, the droplet contour, locus of the focal spot, and the droplet center of mass.

The effective birefringence that results from radial SB can be estimated from phase delay $\Psi$ between ordinary and extraordinary waves passing through the droplet at a distance $\ell$ from its center [see Fig. 5(b)]. We get

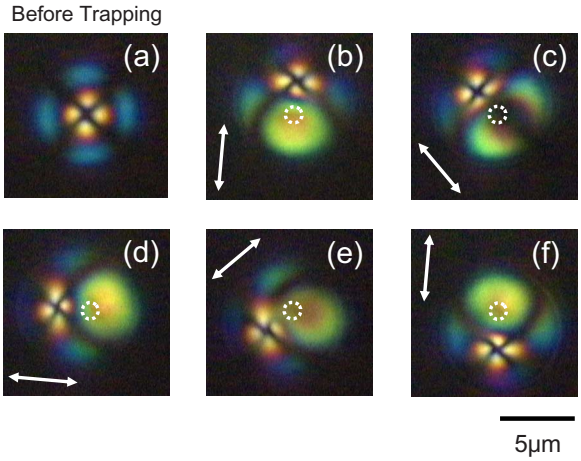


FIG. 4. (Color online) Polariscope images of a 8.1-$\mu$m-diam radial droplet at different orientation of linear polarization (marked by arrows). Panel (a): before trapping; panels (b)–(f): trapping power $P=310$ mW. The dashed circle indicates the locus of the focal spot.

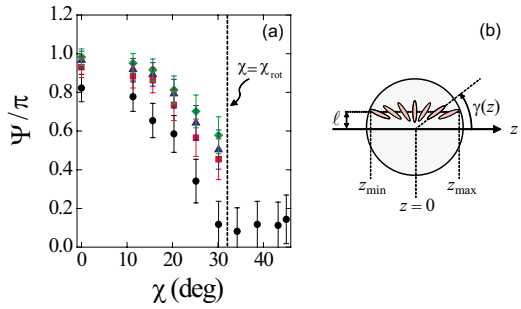


FIG. 5. (Color online) (a) Stationary phase delay $\Psi$ as a function of ellipticity at trapping power $P=62$ mW (circles), $P=186$ mW (squares), $P=310$ mW (triangles), and $P=432$ mW (diamonds) for the situation that corresponds to Fig. 2. (b) Illustration of the corresponding geometry.

$$\Psi = \frac{2\pi}{\lambda}\int_{-R\cos\gamma_0}^{R\cos\gamma_0}\left[\left(\frac{\epsilon_\parallel\epsilon_\perp}{\epsilon_\perp + \epsilon_a\cos^2\gamma(z)}\right)^{1/2} - \epsilon_\perp^{1/2}\right]dz, \quad (1)$$

where $\gamma(z)=\arctan(\ell/z)$, $\gamma_0=\arcsin(\ell/R)$, and $R=d/2$ is the droplet radius. As an example, Fig. 5(a) shows the result for the data presented in Fig. 3. This corresponds to an effective birefringent plate with thickness $d$ having an effective birefringence

$$\Delta n_{\text{eff}} = \frac{\lambda\Psi}{2\pi d}. \quad (2)$$

Typically, the observations reported in Figs. 3 and 5 correspond to the range $0.01<\Delta n_{\text{eff}}<0.08$. More precisely, we can estimate the effective birefringence at $\chi=\chi_{\text{rot}}$ above which the droplet rotates. From the data that correspond to Figs. 2, 3, and 5 we find $\Delta n_{\text{eff}}|_{\chi=\chi_{\text{rot}}}=0.045\pm0.005$, which offers a qualitative explanation for the value $\Delta n_{\text{eff}}|_{\chi=\chi_{\text{rot}}}\simeq 0.022\pm0.015$ obtained from rotational switch-on experiments [17].

### 2. Left-right symmetry breaking

In the elliptical case we observe a twisted Maltese cross, as shown in Figs. 2(c) and 2(d). The sign of such left-right SB is unambiguously related to the handedness of the elliptical polarization and is the signature of a spin angular momentum deposition from the laser beam to the LC. This implies that light must undergo polarization changes, i.e., to experience an overall birefringence, which is the case since $\ell\neq 0$.

In order to quantify the left-right SB effects we define the twist angle $\beta$ of the Maltese cross as depicted in the upper panels of Fig. 6. The effect increases monotonously with power as demonstrated in Fig. 6(a) where the dependence of $\beta$ on the normalized power $P/P_{\text{rot}}$ is shown when polarization is circular, where $P_{\text{rot}}$ is the power above which continuous rotation of the droplet takes place (see the gray region in Fig. 2). We find that the twisting effect has a nonlinear behavior with respect to the trapping power. This can be understood recalling that the spin angular momentum transfer from light to LC depends both on the number of photons passing through the droplet and the local birefringence,

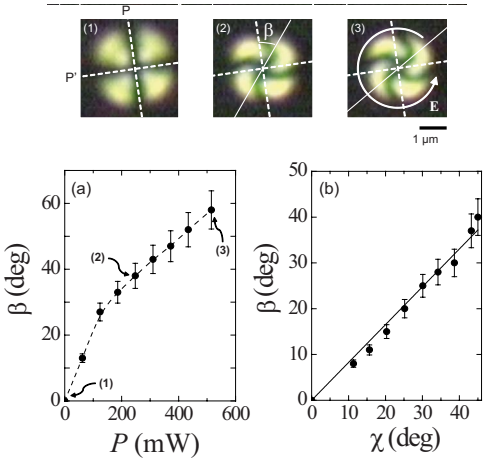


FIG. 6. (Color online) (a) Power dependence of the laser-induced static twist amplitude for a 3.5-$\mu$m diam droplet below the rotation threshold when light is circularly polarized. Upper panels: illustration of the twist angle $\beta$ for polariscope images of a 3.5-$\mu$m-diam droplet, where $P$ and $P'$ refer to the main axes of the crossed polarizers at trapping power $P=0$ (1), 248 (2), and 515 mW (3). The handedness of the circularly polarized tweezers is indicated in panel (3) and the dashed line is a guide for the eye. (b) Ellipticity dependence of the laser-induced static twist amplitude for a 6-$\mu$m-diam droplet below at $P=62$ mW that corresponds to Fig. 2. The solid line is linear fit.

which is actually power dependent. On the other hand, the twist angle dependence on $\chi$ is found to be linear within a good approximation following $\beta=0.83\chi$, as shown in Fig. 6(b).

Left-right SB is observed without rotation of the droplet although angular momentum transfer occurs inside the droplet. In fact there is no contradiction because rotation is driven by the total angular momentum exchange while twisted deformations are related to the gradient of angular momentum exchanges. A stationary time-independent twisted reordering can exist if the reorientation is such that the overall balance of angular momentum is zero. A well-known example is the case of birefringent bipolar nematic liquid-crystal droplets in circularly polarized tweezers, where no rotation is observed below $\chi=\chi_{\text{rot}}$ [13]. By analogy, the critical value $\chi_{\text{rot}}$ for an off-centered radial droplet with $\ell\neq 0$ can be estimated following Ref. [21] by considering the radial droplet as a birefringent plate with effective birefringence given by Eq. (2). The optical torque along $z$ thus writes [21]

$$\Gamma_{\text{opt},z} = \frac{P}{\omega}[\sin 2\chi(1-\cos\Psi) - \cos 2\chi\sin 2\phi\sin\Psi], \quad (3)$$

where $\omega$ is the light frequency and $\phi$ is the angle between the polarization ellipse major axis (i.e., the $x$ axis) and the local extraordinary axis, which is given by the projection of the director onto the $(x,y)$ plane $\mathbf{n}_\perp$, as sketched in Fig. 7. The first term corresponds to the contribution of spin angular momentum deposition that tends to make the director rotate around the $z$ axis while the second term is the restoring contribution that tends to align the director along the $x$ axis (see Fig. 7). For linear polarization, only the restoring term acts

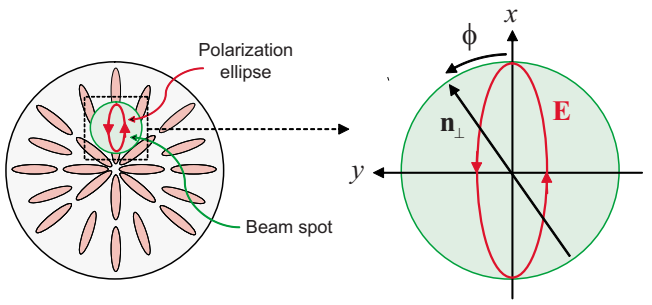


FIG. 7. (Color online) Illustration of the origin of the twisted distortion deformation of an off-centered radial droplet under elliptically polarized laser tweezers.

and imposes $\phi=0$ as a stable fixed position. For elliptical polarization, the competition between the two opposite contributions can lead to a stationary stable position $\phi\neq 0$ if the ellipticity is not too high. The corresponding solution writes $\sin 2\phi=\tan 2\chi\frac{1-\cos\Psi}{\sin\Psi}$ and holds for $\chi<\chi_{\rm rot}$ where $\chi_{\rm rot}$ satisfies

$$\tan 2\chi_{\rm rot}=\frac{\sin\Psi_{\rm rot}}{1-\cos\Psi_{\rm rot}}. \tag{4}$$

The above statements explain the experimentally observed relationship between the twisted Maltese cross and the polarization handedness since $\phi\sim\beta$ is qualitatively expected. Namely, $\beta>0$ for left-handed elliptical polarization (see Fig. 6) and $\beta<0$ for right-handed elliptical polarization (see Fig. 2). In addition, such an estimation of $\chi_{\rm rot}$ can be confronted to experimental observations performed for various droplet diameters shown in Fig. 8(a). Using Eq. (4) and the linear fit of $\chi_{\rm rot}(d)$ [dashed line in Fig. 8(a)] we calculate the diameter dependence of the phase delay $\Psi_{\rm rot}$ as shown in Fig. 8(b). Then we extract the diameter dependence of the associated off-centering length $\ell_{\rm rot}(d)$ by solving Eq. (1). We calculate $\ell_{\rm rot}/d=0.11\pm0.02$ while $\ell_{\rm rot}/d\simeq 0.06$ is observed, from which we conclude to a qualitative agreement only.

Moreover, the absence of rotational dynamics at small power (see Fig. 2 at $P=62$ mW), whatever the polarization is, probably deserves further study. On the one hand, since the center of the trap is located near the glass coverslip there could be some strong wall-droplet interaction [42] preventing rotation at low power, however, we do not have evidence

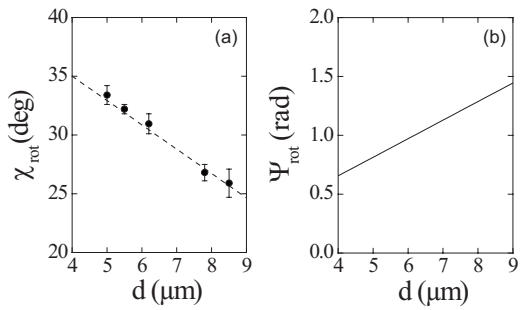


FIG. 8. (a) Experimental $\chi_{\rm rot}$ as a function of the droplet diameter at $P=500$ mW, where the dashed line is linear fit. (b) Calculated $\Psi_{\rm rot}$ as a function of the droplet diameter.

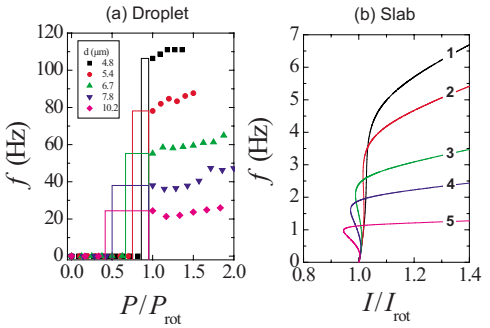


FIG. 9. (Color online) (a) Power dependence of the laser-induced rotation frequency of droplets with various diameter (see the inset) when light is circularly polarized. The bars indicate the intermittent rotation region. (b) Calculated slab analog where the curves (1)–(5) refer, respectively, to the same values of $d$ as in (a).

of it. On the other hand, the almost zero off-centering length measured at large ellipticity values (Fig. 3) perhaps merely indicates the absence of distortion, which in turn explains the absence of rotation.

### B. Dynamics

The optically induced dynamics of 5CB radial droplets in heavy water is next compared with reorientation dynamics of LC molecules in the slab analog as illustrated in Fig. 1. We further discuss the case of circular and elliptical polarization separately.

#### *1. Circular polarization*

When laser tweezers is circularly polarized, stable rotational motion of radial droplets is observed above $P=P_{\rm rot}$. Below that threshold and in the range $P_{\rm inter}<P<P_{\rm rot}$ the droplets are neither continuously rotating nor immobile and an intermittent rotational behavior is observed. Observations for droplets with various diameter are summarized in Fig. 9(a) where $f$ is the rotation frequency determined from power temporal oscillations of the $x$-polarized component of the output light, $P_x(t)$, and the bars indicate the intermittent rotation range. The dependence of $P_{\rm inter,rot}$ as a function of droplet diameter is reported in Fig. 10(a). A critical diameter $d_c$ below which the intermittent region vanishes, i.e., $P_{\rm inter}=P_{\rm rot}$, can be defined. The rotational dynamics for the slab analog is presented in Figs. 9(b) and 10(b) and allows for a qualitative understanding of the main observed features.

First, the rotation threshold $P_{\rm rot}$ may be associated with the optical Fréedericksz transition threshold for the slab where the sudden rotational motion results from a sudden light-induced birefringence $\Psi$ and subsequent spin angular momentum transfer, as shown by curves 2 and 3 of the inset of Fig. 10(b). Second, the intermittent rotation regime may be viewed as the signature of the predicted uniform rotation hysteresis. More quantitatively, $1/d^{\alpha}$ power-law fits of $P_{\rm inter,rot}$ experimental behavior give $\alpha_{\rm inter}=1.86\pm0.21$ and $\alpha_{\rm rot}=0.90\pm0.12$ while slab analog behaves to a good approximation as $\alpha=2$ according to the $1/d^2$ behavior of the Fréedericksz threshold [23]. Such a discrepancy should be explained recalling that the off-centered droplet in laser

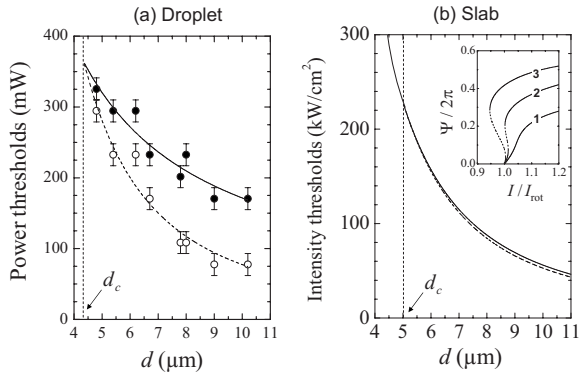


FIG. 10. (a) Droplet diameter dependence of the power thresholds $P_{\text{inter}}$ (open circles) and $P_{\text{rot}}$ (filled circles) as defined in the text when light is circularly polarized. (b) Calculated slab analog where solid and dashed lines correspond to the predicted uniform rotation switch on and off, respectively. Inset: reorientation diagram where the curves (1–3) refer to $d$=4, 6, and 10 $\mu$m and $\Psi$ is the light-induced phase delay.

tweezers breaks the azimuthal symmetry and adds an imperfect character to the Fréedericksz transition that is not taken into account in present simulations. Finally, the occurrence of a monovalued reorientation diagram [see the inset of Fig. 10(b), curve 1] for small $d$ in the slab analog defines a critical value $d_c \simeq 5.0$ $\mu$m which is close to the value $d_c \simeq 4.4$ $\mu$m extrapolated from experimental data as the intersection of the power-law fits [see Fig. 10(a)]. Finally, the observed rotation frequency locking above $P_{\text{rot}}$ [see Fig. 9(a)] proves the complex character of the light-induced reorientation inside the droplet. Indeed it means that the induced birefringence has a strongly nonlinear power behavior, which is known to be associated with the excitation of twisted reorientation modes in the slab case [36].

### 2. Elliptical polarization

Droplet rotation using elliptically polarized tweezers is summarized in Fig. 11(a) where the rotation frequency is

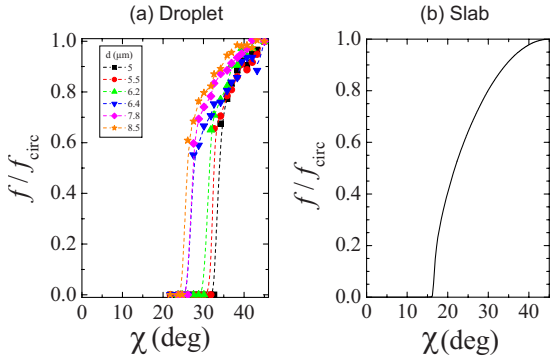


FIG. 11. (Color online) (a) Polarization dependence of the normalized laser-induced rotation frequency of droplets with various diameter (see the inset) at trapping power $P$=500 mW where $f_{\text{circ}}$ is the rotation frequency for circular polarization ($\chi$=45°). The dashed line is a guide for the eye. (b) Calculated slab analog for $d$=5 $\mu$m.

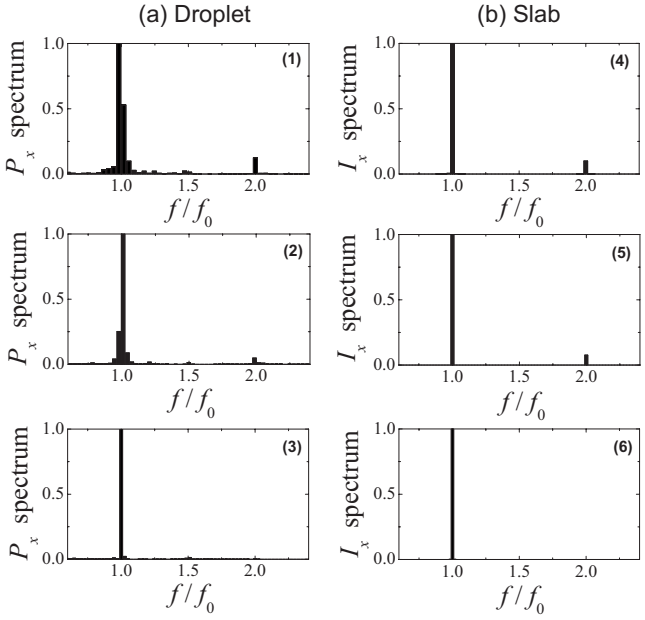


FIG. 12. (a) Polarization dependence of the Fourier power spectra of the $x$-polarized output light intensity for a 5.5-$\mu$m-diam droplet at trapping power $P$=500 mW where the frequency is normalized to the rotation fundamental frequency $f_0$. Panels (1)–(3) refer to $\chi$=34.2°, 36.9°, and 45°. (b) Calculated slab analog for $d$=5 $\mu$m. Panels (4)–(6) refer to $\chi$=25°, 30°, and 45°.

plotted as a function of ellipticity for various diameters at a fixed power $P$=500 mW. Abrupt frequency changes as a function of $\chi$ are observed in a tiny range around $\chi_{\text{rot}}$ and indicate, at least, abrupt changes of the light-induced birefringence. The calculated behavior for slab analog with $d$=5 $\mu$m shown in Fig. 11(b) also predict abrupt, but continuous, frequency changes. There we fixed $I/I_{\text{rot}} \simeq 1.6$ in agreement with the experimental value $P/P_{\text{rot}}$ deduced from Fig. 9(a). In fact the apparent jump observed experimentally may be explained from finite ellipticity increment $\delta\chi$ used in practice, namely, $0.8° < \delta\chi < 1.7°$. For example, from $\delta\chi$ =1.6° at $d$=5 $\mu$m we estimate a jump $\delta f/f_{\text{circ}} \simeq 0.25$ which gives the correct order of magnitude.

Then we have explored the nonlinear character of the rotational dynamics under elliptically polarized excitation beam, recalling that homeotropic slabs are known to exhibit nonlinear rotations under elliptically polarized beams [37]. For this purpose, we performed the fast Fourier transform analysis of $P_x(t)$ experimental data and compared it with calculations for the slab analog. The results are presented in Fig. 12. The nonuniform rotation for almost circular polarization was experimentally observed as shown in Fig. 12(a) where $2f_0$ harmonics is observed for $\chi < 45°$ [see panels (1) and (2)] in contrast to uniform rotation for circular polarization [see panel (3)]. This is in good correspondence with the slab prediction shown in Fig. 12(b) where the second harmonic vanishes at $\chi$=45° [see panels (4)–(6)].

## IV. CONCLUSION

We have studied statics and dynamics of radial nematic liquid-crystal droplets manipulated by linearly, elliptically, or

circularly polarized laser tweezers. Static in-plane or twisted deformation modes and steady or unsteady nonlinear rotational dynamics are observed. The role of symmetry breaking and molecular reordering has been identified and is shown to depend both on trapping power and tweezers polarization. Radial symmetry breaking occurs whatever the polarization is whereas left-right symmetry breaking is associated with the angular momentum carried by the tweezers. The intensity dependence of symmetry breaking effects is related to optically induced reordering of the droplets. The results are compared with the corresponding slab analog, for which orientational optical nonlinearities effects can be described quantitatively with accuracy. Qualitative agreement between simulations and observations is obtained and points out the main ingredients of light-induced liquid-crystal bulk reordering in a confined geometry.

## ACKNOWLEDGMENTS

Partial financial support by an international collaboration grant from RIES, Hokkaido University and the Grant-in-Aid from the Ministry of Education, Science, Sports, and Culture of Japan Grant No. 19360322 are acknowledged.

[1] A. Ashkin, Phys. Rev. Lett. **24**, 156 (1970).
[2] A. Ashkin, Proc. Natl. Acad. Sci. U.S.A. **94**, 4853 (1997).
[3] D. G. Grier, Nature (London) **424**, 810 (2003).
[4] K. C. Neuman and S. M. Block, Rev. Sci. Instrum. **75**, 2787 (2004).
[5] H. Misawa and S. Juodkazis, Prog. Polym. Sci. **24**, 665 (1999).
[6] S. Juodkazis, N. Mukai, R. Wakaki, A. Yamaguchi, S. Matsuo, and H. Misawa, Nature (London) **408**, 178 (2000).
[7] D. McGloin, Philos. Trans. R. Soc. London, Ser. A **364**, 3521 (2006).
[8] J. E. Molloy and M. J. Padgett, Contemp. Phys. **43**, 241 (2002).
[9] P. Galajda and P. Ormos, Appl. Phys. Lett. **78**, 249 (2001).
[10] M. P. MacDonald, G. C. Spalding, and K. Dholakia, Nature (London) **426**, 421 (2003).
[11] Y. Nabetani, H. Yoshikawa, A. C. Grimsdale, K. Müllen, and H. Masuhara, Langmuir **23**, 6737 (2007).
[12] S. J. Woltman, G. D. Jay, and G. P. Crawford, Nat. Mater. **6**, 929 (2007).
[13] S. Juodkazis, S. Matuso, N. Murazawa, I. Hasegawa, and H. Misawa, Appl. Phys. Lett. **82**, 4657 (2003).
[14] T. A. Wood, H. F. Gleeson, M. R. Dickinson, and A. J. Wright, Appl. Phys. Lett. **84**, 4292 (2004).
[15] N. Murazawa, S. Juodkazis, and H. Misawa, Eur. Phys. J. E **20**, 435 (2006).
[16] H. F. Gleeson, T. A. Wood, and M. Dickinson, Philos. Trans. R. Soc. London, Ser. A **364**, 2789 (2006).
[17] N. Murazawa, S. Juodkazis, and H. Misawa, J. Phys. D **38**, 2923 (2005).
[18] F. Xu, H.-S. Kitzerow, and P. P. Crooker, Phys. Rev. A **46**, 6535 (1992).
[19] F. Xu, H.-S. Kitzerow, and P. P. Crooker, Phys. Rev. E **49**, 3061 (1994).
[20] F. Xu and P. P. Crooker, Phys. Rev. E **56**, 6853 (1997).
[21] M. E. J. Friese, T. A. Nieminen, N. R. Heckenberg, and H. Rubinsztein-Dunlop, Nature (London) **394**, 348 (1998).
[22] A. Yu. Savchenko, N. V. Tabiryan, and B. Ya. Zel'dovich, Phys. Rev. E **56**, 4773 (1997).
[23] N. V. Tabiryan, A. V. Sukhov, and B. Ya. Zel'dovich, Mol. Cryst. Liq. Cryst. **136**, 1 (1986).
[24] N. Murazawa, S. Juodkazis, S. Matuso, and H. Misawa, Small **1**, 656 (2005).
[25] N. Murazawa, S. Juodkazis, V. Jarutis, Y. Tanamura, and H. Misawa, Europhys. Lett. **73**, 800 (2006).
[26] N. Murazawa, S. Juodkazis, Y. Tanamura, and H. Misawa, Jpn. J. Appl. Phys., Part 1 **45**, 977 (2006).
[27] S. Juodkazis, M. Shikata, T. Takahashi, S. Matuso, and H. Misawa, Appl. Phys. Lett. **74**, 3627 (1999).
[28] T. A. Wood, G. S. Roberts, S. Eaimkhong, and P. Bartlett, Faraday Discuss. **137**, 319 (2008).
[29] C. Manzo, D. Paparo, L. Marrucci, and I. Jánossy, Phys. Rev. E **73**, 051707 (2006).
[30] J. Hotta, K. Sasaki, and H. Masuhara, Appl. Phys. Lett. **71**, 2085 (1997).
[31] A. Pattanaporkratana, C. S. Park, J. E. Maclennan, and N. A. Clark, Ferroelectrics **310**, 131 (2004).
[32] I. I. Smalyukh, B. I. Senyuk, S. V. Shiyanovskii, O. D. Lavrentovich, A. N. Kuzmin, A. V. Kachynski, and P. N. Prasad, Mol. Cryst. Liq. Cryst. **450**, 79 (2006).
[33] I. I. Smalyukh, D. S. Kaputa, A. V. Kachynski, A. N. Kuzmin, and P. N. Prasad, Opt. Express **15**, 4359 (2007).
[34] Y. Iwashita and H. Tanaka, Phys. Rev. Lett. **90**, 045501 (2003).
[35] I. I. Smalyukh, A. V. Kachynski, A. N. Kuzmin, and P. N. Prasad, Proc. Natl. Acad. Sci. U.S.A. **103**, 18048 (2006).
[36] E. Brasselet, T. V. Galstian, L. J. Dubé, D. O. Krimer, and L. Kramer, J. Opt. Soc. Am. B **22**, 1671 (2005).
[37] D. O. Krimer, L. Kramer, E. Brasselet, T. V. Galstian, and L. J. Dubé, J. Opt. Soc. Am. B **22**, 1681 (2005).
[38] E. Santamato, B. Daino, M. Romagnoli, M. Settembre, and Y. R. Shen, Phys. Rev. Lett. **57**, 2423 (1986).
[39] E. Santamato, G. Abbate, P. Maddalena, L. Marrucci, and Y. R. Shen, Phys. Rev. Lett. **64**, 1377 (1990).
[40] L. Marrucci, G. Abbate, S. Ferraiuolo, P. Maddalena, and E. Santamato, Phys. Rev. A **46**, 4859 (1992).
[41] A. Vella, B. Piccirillo, and E. Santamato, Phys. Rev. E **65**, 031706 (2002).
[42] M. Miwa, S. Juodkazis, and H. Misawa, Jpn. J. Appl. Phys., Part 1 **39**, 1930 (2000).